






Article

Electrochemical Study of Nd and Pr Co-Deposition onto Mo and W from Molten Oxyfluorides

Vesna S. Cvetković ^{1,*} , Dominic Feldhaus ², Nataša M. Vukićević ¹ , Tanja S. Barudžija ³ , Bernd Friedrich ² 
and Jovan N. Jovićević ¹ 

¹ Department of Electrochemistry, Institute of Chemistry, Technology and Metallurgy, National Institute, University of Belgrade, Njegoševa 12, 11000 Belgrade, Serbia; vukicevic@ihm.bg.ac.rs (N.M.V.); jovicovic@ihm.bg.ac.rs (J.N.J.)

² IME Process Metallurgy and Metal Recycling, Institute of RWTH Aachen University, Intzestr. 3, 52056 Aachen, Germany; DFeldhaus@metallurgie.rwth-aachen.de (D.F.); BFriedrich@metallurgie.rwth-aachen.de (B.F.)

³ Institute for Nuclear Sciences Vinča, University of Belgrade, P.O. Box 522, 11001 Belgrade, Serbia; tbarudzija@vin.bg.ac.rs

* Correspondence: v.cvetkovic@ihm.bg.ac.rs

Abstract: Electrodeposition processes of neodymium and praseodymium in molten $\text{NdF}_3 + \text{PrF}_3 + \text{LiF} + 1 \text{ wt.}\% \text{Pr}_6\text{O}_{11} + 1 \text{ wt.}\% \text{Nd}_2\text{O}_3$ and $\text{NdF}_3 + \text{PrF}_3 + \text{LiF} + 2 \text{ wt.}\% \text{Pr}_6\text{O}_{11} + 2 \text{ wt.}\% \text{Nd}_2\text{O}_3$ electrolytes at 1323 K were investigated. Cyclic voltammetry, square wave voltammetry, and open circuit potentiometry were applied to study the electrochemical reduction of Nd(III) and Pr(III) ions on Mo and W cathodes. It was established that a critical condition for Nd and Pr co-deposition in oxyfluoride electrolytes was a constant praseodymium deposition overpotential of $\approx -0.100 \text{ V}$, which was shown to result in co-deposition current densities approaching 6 mAcm^{-2} . Analysis of the results obtained by applied electrochemical techniques showed that praseodymium deposition proceeds as a one-step process involving exchange of three electrons ($\text{Pr(III)} \rightarrow \text{Pr(0)}$) and that neodymium deposition is a two-step process: the first involves one electron exchange ($\text{Nd(III)} \rightarrow \text{Nd(II)}$), and the second involves an exchange of two electrons ($\text{Nd(II)} \rightarrow \text{Nd(0)}$). X-ray diffraction analyses confirmed the formation of metallic Nd and Pr on the working substrate. Keeping the anodic potential to the glassy carbon working anode low results in very low levels of carbon oxides, fluorine and fluorocarbon gas emissions, which should qualify the studied system as an environmentally friendly option for rare earth metal deposition. The newly reported data for Nd and Pr metals co-deposition provide valuable information for the recycling of neodymium-iron-boron magnets.

Keywords: neodymium; praseodymium; electrodeposition; fluoride melts; gas emission: SWV; XRD



Citation: Cvetković, V.S.; Feldhaus, D.; Vukićević, N.M.; Barudžija, T.S.; Friedrich, B.; Jovićević, J.N. Electrochemical Study of Nd and Pr Co-Deposition onto Mo and W from Molten Oxyfluorides. *Metals* **2021**, *11*, 1494. <https://doi.org/10.3390/met11091494>

Academic Editor: Caterina Zanella

Received: 26 August 2021

Accepted: 17 September 2021

Published: 21 September 2021

Publisher's Note: MDPI stays neutral with regard to jurisdictional claims in published maps and institutional affiliations.



Copyright: © 2021 by the authors. Licensee MDPI, Basel, Switzerland. This article is an open access article distributed under the terms and conditions of the Creative Commons Attribution (CC BY) license (<https://creativecommons.org/licenses/by/4.0/>).

1. Introduction

The growing demand for neodymium–iron–boron permanent magnets ($\text{Nd}_2\text{Fe}_{14}\text{B}$, or NdFeB), driven particularly by their use in wind turbines, high-tech products, etc., requires an ever increasing supply of rare earth based materials [1–5]. An NdFeB magnet, depending on the application, contains about 31–32 wt.% of rare earth elements (REEs), mainly neodymium and praseodymium (Nd + Pr) [6]. The combination of the supply shortage of rare earth minerals and increasing supply of rare earth solid wastes calls for a simple, inexpensive, and environmentally friendly recycling process for REEs in order to supplement current supply chains.

Interest in the recovery of the rare earth metals neodymium and praseodymium from their secondary sources, mainly from the end-of-life NdFeB magnet scrap, is becoming increasingly important for the sustainable rare earth industry [1,4,7]. Most of the recycling processes are in their development stages and require technology advances to achieve sustainable production. To find a solution for the growing environmental problems and

to ensure the sustainable production of these materials in the future, electrometallurgy, especially molten salt electrolysis, offers great potential. Advantages such as high purity of end product, low energy consumption, and high efficiency have already been reported in the electrolytic production process of Nd-Pr alloys [8]. Separation of neodymium from praseodymium is rather difficult because of their similarity in terms of either their chemical properties or their occurrence in rare earth minerals in nature. As a result, in some applications, such as permanent magnets, the term didymium (Di), which is an Nd-Pr alloy, is used [8]. For deposition processing of neodymium and praseodymium via molten salt electrolysis, in terms of efficiency and environmental footprint, molten fluorides or chlorides are commonly used as electrolytes [8–12].

A series of studies have been successfully performed to determine not only the electrochemical behaviour of Nd or Pr in different electrolyte media, but also to obtain RE metal alone or RE-alloy samples by selective electrochemical deposition on chosen working substrates [11–16]. Nevertheless, the processes for Nd-Pr alloy production by electrolysis from molten chloride or fluoride were difficult to execute and only limited research has been published [17,18].

Yasuda et al. reported the electrochemical separation of Pr, Nd, and Dy from used magnet scrap by potentiostatic electrolysis using Ni plate in a molten NaCl-KCl-NdCl₃-DyCl₃ and NaCl-KCl-PrCl₃-NdCl₃-DyCl₃ at 973 K [19]. However, using a molten fluoride salt electrolyte instead of chloride is expected to provide advantages such as higher current efficiencies, lower hygroscopicity and higher conductivity [20,21].

The fluoride molten salt system, which is usually based on a mixture of a rare earth fluoride and an alkali metal fluoride, is employed as both a solvent for neodymium oxide/praseodymium oxide and an electrolyte for the electrolytic production of Nd-Pr alloys [8,18,22]. Initially, Morrice et al. in a study reported in the 1960s, obtained high purity rare earth metals, neodymium, praseodymium and didymium by electrowinning from the electrolyte composed of appropriate rare earth fluoride (neodymium or praseodymium fluoride), lithium fluoride and rare earth oxide, and these studies remain a relevant reference to now [23]. Yang et al. focused on the selective dissolution of an anode made of rare earth permanent magnet (REPM) waste into molten LiF-CaF₂ salts [17]. The resulting Nd and Pr ions were then directly reduced to individual rare earth metals and then formed alloys with the cathode substrate by electrolysis [17]. Milicevic et al. also studied the synthesis of neodymium and praseodymium, including perfluorocarbon emission from oxide-fluoride molten salts by electrolysis [24,25].

Despite the efforts made so far, there are still a number of remaining challenges, mainly concerned with the composition of the electrolytes based on neodymium, praseodymium, lithium fluorides and neodymium and praseodymium oxides and their influence on all aspects of desired effective rare earth metals electrodeposition.

This study aims to take the next step towards better understanding the electrochemical reduction of neodymium(III) and praseodymium(III) ions on the chosen inert cathode in the oxide fluoride molten salt electrolyte. More specifically, the reaction mechanism of neodymium and praseodymium deposition from fluoride based molten salts containing different ratios of rare earth oxides will be studied, in order to provide an optimum electrodeposition potential for larger Nd and Pr metal deposits on the cathode surface and to minimize the evolution of perfluorocarbon gases from the system.

2. Materials and Methods

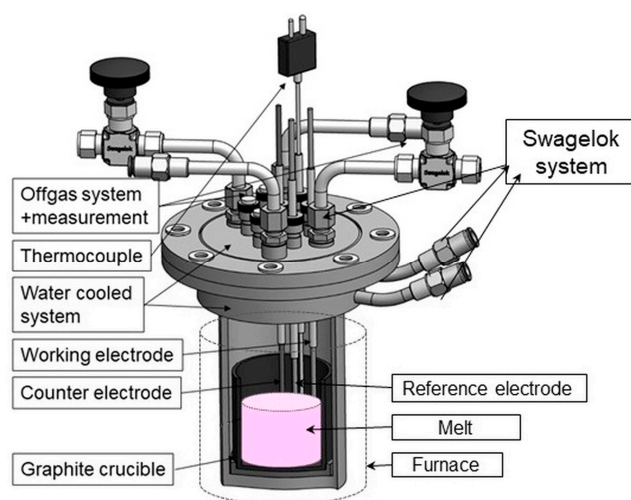
The used electrolytes were composed of neodymium fluoride (NdF₃, ≥99.9%), praseodymium fluoride (PrF₃, ≥99.9%), lithium fluoride (LiF, ≥99.5%), neodymium oxide (Nd₂O₃, ≥99.9%) and praseodymium oxide (Pr₆O₁₁, ≥99.9%). All the chemicals were purchased from Treibacher, Althofen, Austria. Two electrolytes were developed. The composition of each was as shown in Table 1. The key composition difference is in the oxide concentration. The two oxides made up 2 wt.% of the Electrolyte I and 4 wt.% of the Electrolyte II.

Table 1. Chemical composition of the electrolytes.

The Electrolytes	Component				
	Weight Percentage [%]/Molar Ratio [%]				
	NdF ₃	PrF ₃	LiF	Nd ₂ O ₃	Pr ₆ O ₁₁
Electrolyte I	64.41/35.40	21.37/11.94	12.25/52.23	0.98/0.32	0.98/0.11
Electrolyte II	63.17/35.24	20.96/11.89	12.02/52.02	1.92/0.64	1.92/0.21

Before being manually mixed, the fluorides were dried in a furnace for 24 h at 523 K. Mixed fluorides were melted in a high purity graphite crucible. This process was conducted in a vacuum induction furnace, which operated in overpressure condition in order to counteract the high vapour pressure of the fluorides under 1800 mbar of argon pressure at temperatures up to 1373 K. Before they were added to the electrolyte, neodymium and praseodymium oxides were also dried in a furnace for 24 h at 393 K.

Electrochemical experiments were conducted in a three-electrode steel cell, shown in Figure 1. As working electrodes, 2-mm-diameter, EWG 99.95% molybdenum or tungsten electrodes were used, with surface area of 1 cm² exposed to contact with the melt. The potentials were referenced to the RE, which was made from tungsten (1 mm diameter, EWG 99.95%). The CEs were made from high purity glassy carbon (>99.99% HTW SIGRADUR® G). Glassy carbon as chemically relatively stable compared to other types of carbon materials was chosen to be used in our experiments [26,27]. Prior to insertion in the cell, the surface of the electrodes used was polished thoroughly with SiC emery paper, rinsed with deionized water and ethanol, and dried in open air.

**Figure 1.** Electrochemical cell setup.

The graphite crucible, filled with the salt mixture, was placed into the steel electrochemical cell; the lid was closed, and the cell was placed into a resistance furnace. The working temperature of 1323 K was controlled by a type K thermocouple controller. To protect the seals of the Swagelok system, which makes the swaps of the electrodes during the experiment possible, the lid of the cell must be water-cooled. Thus, the cell operates in an airtight environment, which on one hand prevents the toxic gases from leaking out of the cell and on the other hand prevents the electrolyte from oxidizing. The cell is also kept under argon atmosphere. The exhaust gases were discharged in a controlled manner, washed with sodium hydroxide solution and fed into the exhaust system. A certain amount of the off-gas is taken by the off-gas measurement system—Gasetm DX4000 Fourier transformation infrared spectrometer (FTIR, Ansyco, Karlsruhe, Germany)—for an online analysis displayed every 5 s.

All electrochemical measurements: cyclic voltammetry (CV), chronopotentiometry, square wave voltammetry (SWV) and open circuit chronopotentiometry, were controlled by an IviumStat potentiostat (5 A/10 V; Ivium Technologies Eindhoven, Netherlands). The cyclic voltammograms obtained, started from potential E_I , usually 0.050 V negative to the working electrode open circuit potential (measured against the tungsten reference electrode), changed to a chosen cathodic end potential, E_C , and back with various sweep rates. Long-term experiments were carried out for up to 90 min at constant overpotentials to provide adequate time for the metal to deposit on the working electrode. The surfaces of the samples and deposits were initially examined by an optical microscope (Keyence; model VH-Z100R, Osaka, Japan). Solidified deposits were mechanically removed from the working electrode and subsequently analysed by X-ray diffraction (XRD) with Philips PW 1050 powder diffractometer (Philips, Delft, The Netherlands) at room temperature with Ni filtered $\text{CuK}\alpha$ radiation ($\lambda = 1.54178 \text{ \AA}$), scintillation detector within $20\text{--}85^\circ 2\theta$ range in steps of 0.05° , and scanning time of 5 s per step.

3. Results and Discussion

The cyclic voltammetry technique was used to help identify possible redox reactions taking part on Mo and W working electrodes in both electrolytes. Cathodic end potential, E_C , was gradually swept from the initial potential, E_I , towards more negative values. A typical result is presented in Figure 2. Clear indications of four redox processes were obtained in the potential range up to 1.000 V negative to the open circuit of the working Mo or W electrode in Electrolyte I. They were represented as four reduction (cathodic) current waves (C_1 , C_2 , C_3 and C_4) and four oxidation (anodic) counterparts (A_1 , A_2 , A_3 and A_4). Comparing the current wave peak potentials shown in Figure 2 to the similar current wave potentials obtained in our previous study from $\text{NdF}_3 + \text{LiF} + 2 \text{ wt.}\% \text{Nd}_2\text{O}_3$ electrolyte on W and Mo electrodes under the same conditions for the neodymium deposition and dissolution, helped attribution of C_1/A_1 and C_2/A_2 to the deposition and dissolution of neodymium and C_4/A_4 to the deposition and dissolution of lithium [12,15]. According to the data published in our earlier work, in the fluoride electrolyte, neodymium reduces to the metal form in two steps, seen as C_1 and C_2 in Figure 2 [12,15]. Therefore, the electrode reaction corresponding to the current waves C_3/A_3 can be assigned to possible deposition and dissolution of praseodymium.

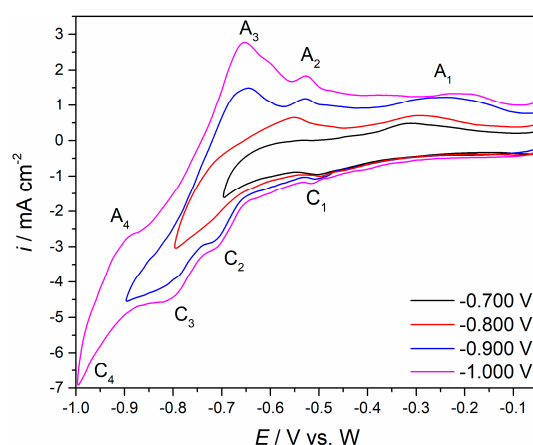


Figure 2. Cyclic voltammograms recorded on W working electrode in $\text{NdF}_3 + \text{PrF}_3 + \text{LiF} + 1 \text{ wt.}\% \text{Pr}_6\text{O}_{11} + 1 \text{ wt.}\% \text{Nd}_2\text{O}_3$ electrolyte, $E_I = -0.050 \text{ V vs. W}$ to different cathodic end potential E_C , obtained with sweep rate of $50 \text{ mV}\cdot\text{s}^{-1}$.

Cyclic voltammetry with different scan rates (50 and $300 \text{ mV}\cdot\text{s}^{-1}$) was employed to study the electrochemical reactions related to Nd and Pr redox transitions on W and Mo working electrodes. Figure 3a,b show voltammograms obtained on each of the working electrode substrates (Mo and W) in the molten Electrolyte I, at 1323 K . On both substrates,

within the applied potential range, the voltammograms, exhibited three distinct current waves C_1 , C_2 and C_3 in the cathodic sections and corresponding anodic counterparts A_1 , A_2 and A_3 in the anodic sections of the scanned potential range.

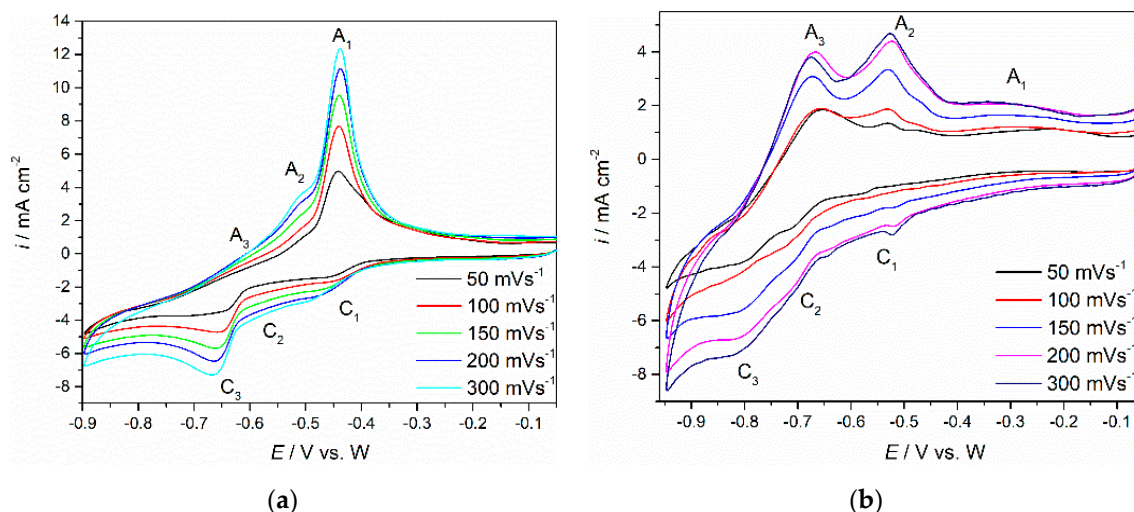


Figure 3. CVs recorded on: (a) Mo working electrode starting from: $E_I = -0.050$ V to $E_C = -0.900$ V vs. W; (b) W working electrode starting from: $E_I = -0.050$ V to $E_C = -0.950$ V vs. W. The voltammograms were obtained with different sweep rates in molten $\text{NdF}_3 + \text{PrF}_3 + \text{LiF} + 1 \text{ wt.}\% \text{Pr}_6\text{O}_{11} + 1 \text{ wt.}\% \text{Nd}_2\text{O}_3$ electrolyte, temperature 1323 K.

Furthermore, it was apparent that there were in fact three redox reactions (C_1/A_1 , C_2/A_2 and C_3/A_3), because each cathodic current wave was a prerequisite for its anodic counterpart.

The small difference between the voltammograms obtained on Mo and W was recorded in the peak potentials of the recorded current waves. On W working electrode, the current wave C_1 , starting at ≈ -0.550 V vs. W, should reflect the reduction of Nd(III) to Nd(II), and the anodic peak A_1 in the reverse scan at ≈ -0.300 V vs. W, should reflect the oxidation of Nd(II) to Nd(III) [12,15,20]. At more cathodic potentials ≈ -0.700 V vs. W, the reduction current wave C_2 should be assigned to further reduction of Nd(II) to Nd(0), and the anodic counterpart current wave A_2 should represent the oxidation of Nd(0) to Nd(II). In other words, the reduction process of Nd(III) ions to Nd metal takes place in two steps, $\text{Nd(III)} \rightarrow \text{Nd(II)}$ and $\text{Nd(II)} \rightarrow \text{Nd(0)}$, which is in accordance with the results reported in molten fluorides with Nd_2O_3 added [12,15,20]. At the potentials negative to -0.700 V vs. W, a third reduction current wave was observed. Since the C_3 current wave potentials are cathodic with respect to the reduction potential of Nd(II), cathodic peak C_3 (starting from around -0.800 V vs. W) should be associated with the electroreduction of Pr(III) to Pr(0). In the anodic scan, starting at around -0.670 V vs. W, the oxidation current wave A_3 , should then correspond to the dissolution of Pr metal that was previously deposited on the working electrode, e.g., $\text{Pr(0)} \rightarrow \text{Pr(III)}$. It appeared that the electroreduction of Pr(III) ions to Pr metal in this system is a single one-step process, $\text{Pr(III)} \rightarrow \text{Pr(0)}$, which is in agreement with the results observed in similar molten fluoride electrolytes [5,17,28]. On the basis of experimental results in this study, the cathodic peak potential values C_2 and C_3 , as seen on CVs in Figure 3a,b, reflecting the electroreduction potentials of Nd(II) ions into Nd metal (C_2), are more positive than the electroreduction potential of Pr(III) ions (C_3), which is consistent with the results seen in the literature [17]. Additionally, due to close values of the reduction potentials for reactions: $\text{Nd(II)} + 2e^- \rightarrow \text{Nd(0)}$, and $\text{Pr(III)} + 3e^- \rightarrow \text{Pr(0)}$, it was difficult to obtain ideally shaped individual current waves by cyclic voltammetry, particularly at higher scan rates. As recorded in voltammograms obtained on Mo and W cathodes, potentials of cathodic current waves on the Mo substrate are slightly shifted toward more positive values compared to the W substrate, whereas the anodic

current waves are similar in values. Therefore, it can be assumed that in the Electrolyte I system, W and Mo working electrodes behave almost identically. Similar results were observed with Mo and W WEs in $\text{NdF}_3 + \text{LiF} + 2 \text{ wt.}\% \text{Nd}_2\text{O}_3$ melts [15].

To investigate the redox reactions further, the CVs recorded at different scan rates on Mo and W electrodes in molten $\text{NdF}_3 + \text{PrF}_3 + \text{LiF} + 1 \text{ wt.}\% \text{Pr}_6\text{O}_{11} + 1 \text{ wt.}\% \text{Nd}_2\text{O}_3$ electrolyte (Figure 3a,b) were recorded and analysed. It was observed that with an increase in scan rates ($50\text{--}300 \text{ mV}\cdot\text{s}^{-1}$), reduction current densities for peaks C_1 , C_2 and C_3 and oxidation current densities for peaks A_3 , A_2 and A_1 increased. Attempts were made to recognize the possible reversibility of the recorded redox reactions or their parts. The reversibility was examined by plotting the influence of the scan rates applied to the current wave peak potentials recorded. Figure 4 shows graphical representations of the plots derived from the data in Figure 3a:

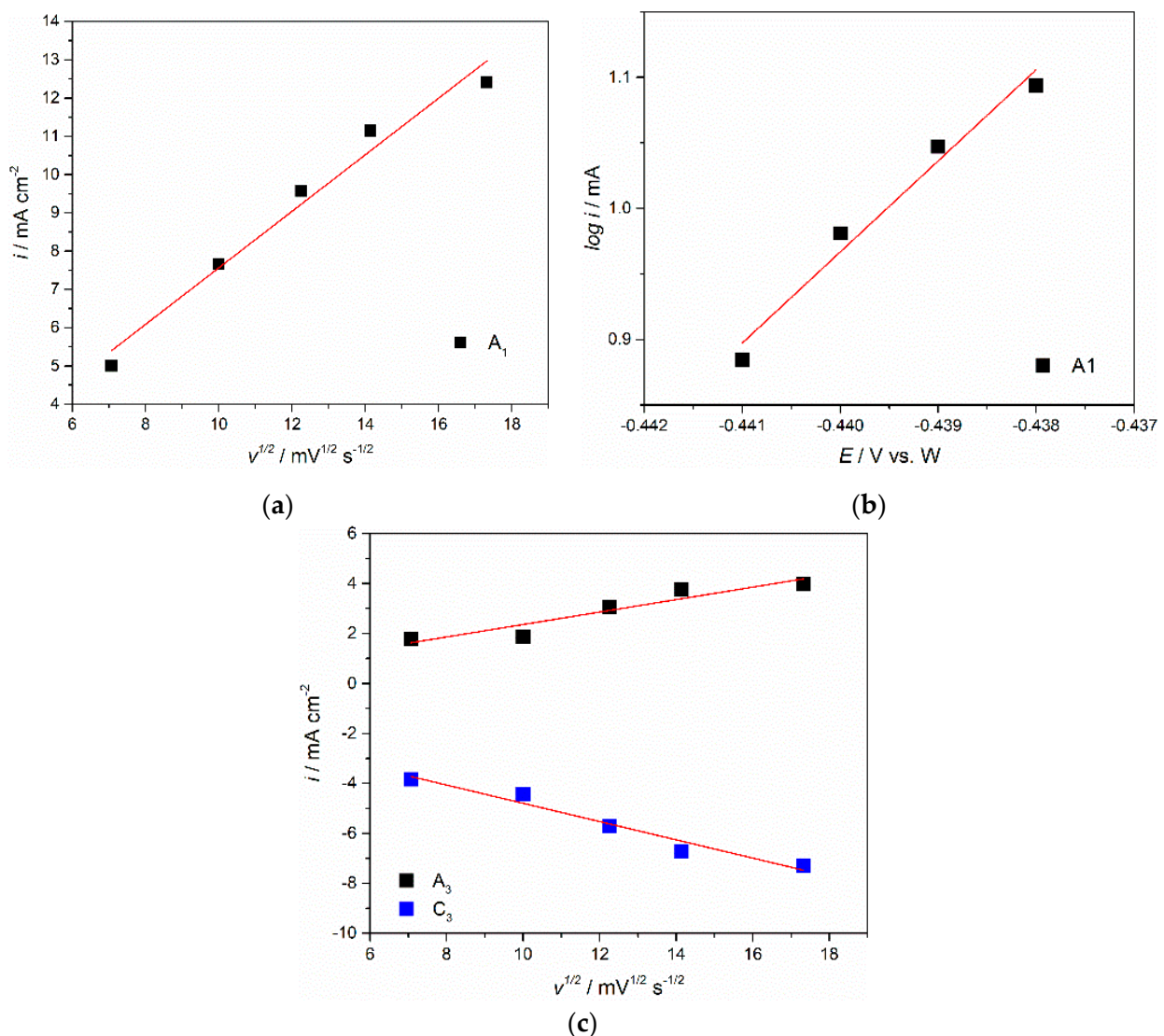


Figure 4. Plots of anodic peak A_1 : (a) current densities vs. square root of scan rate calculated from Figure 3a; (b) logarithm of the peak current density vs. peak potential from the same anodic peak in Figure 3a; (c) plots of peaks A_3/C_3 , anodic and cathodic peak current densities vs. square root of scan rates derived from Figure 3b.

(a) A_1 anodic peak current density values as a function of square root of the scan rates applied, and (b) the logarithms of A_1 anodic peak current values as a function of the peak potentials recorded for different potential scan rates applied ($\log i_p = f(E_p)$). The first plot appears to be linear and does not pass through the origin, Figure 4a. This should indicate that the oxidation process $\text{Nd(II)} \rightleftharpoons \text{Nd(III)}$ is reversible and under mixed control, as was shown in the earlier work done in neodymium oxyfluoride melts under very similar conditions [12,15,20]. The relationship presented in Figure 4b is linear for the whole range of the scan rates applied, which made it possible for the number of exchanged electrons in the $\text{Nd(II)} \rightarrow \text{Nd(III)}$ reaction to be calculated. The calculation was performed using the equation often employed in electrodeposition studies that defining the slope (K) as a function of $\log i_p = f(E_{\text{PEAK}})$ and the number of electrons involved in the reaction (z) [12,15,20]. It was found that the slope K of the linear function from Figure 4b was 2.39, and the corresponding electron transfer number therefore should be 1.25, so close to 1. This directly confirmed the oxidation reaction recorded as an oxidation process A_1 (Figure 3a) involves one electron exchange in electrochemical oxidation of Nd(II) to Nd(III) . Thus, it was confirmed that the redox reaction reflected as a current wave pair C_1/A_1 was $\text{Nd(II)} \rightleftharpoons \text{Nd(III)}$, which nominated the current wave pair C_2/A_2 as the $\text{Nd(II)} \rightleftharpoons \text{Nd(0)}$ as a redox reaction [12,20].

The data presented in Figure 4c, where the maximum cathodic current densities for peak C_3 and its anodic counterpart peak A_3 from Figure 3b are plotted versus the square root of the scan rates applied, indicated a linear relationship that did not pass through the origin. The results were implying that the redox process recorded as the C_3/A_3 current wave pair ($\text{Pr(III)} \rightleftharpoons \text{Pr(0)}$) was reversible and under mixed control: by mass transfer of the complexed praseodymium ions in the molten $\text{NdF}_3 + \text{PrF}_3 + \text{LiF} + 1 \text{ wt.}\% \text{Pr}_6\text{O}_{11} + 1 \text{ wt.}\% \text{Nd}_2\text{O}_3$ and that the rate of the charge transfer step was likely complicated by the dismantling structure of the praseodymium oxyfluoride complexes [25,29].

Although values of the peak potentials for the redox pairs C_3/A_3 , C_2/A_2 and C_1/A_1 in the voltammograms, Figure 3a,b, were slightly different from when the scan rates applied were varied, the observed should be attributed to the reversible reactions under mixed control as shown above and in our previous studies [12,15]. These conclusions apply for both Mo and W working electrodes.

CV performed on Mo electrode in the same molten fluoride while applying different holding times at chosen cathodic end potentials, $E_C = -0.630 \text{ V vs. W}$, before returning to the starting potential, E_I , is shown in Figure 5. C_2/A_2 and C_1/A_1 identify the redox signals that occurred within this potential window. The same electrochemical reactions associated with C_2/A_2 and C_1/A_1 redox couples were observed in previous studies and described as neodymium electrochemical deposition/dissolution in two steps on/from Mo working electrode under given conditions [12,15,20]. In a separate set of experiments, the cathodic end potential of the Mo working electrode was held at -0.850 V vs. W , Figure 6a, and the W working electrode at -0.900 V vs. W , Figure 6b, for 60, 180 and 300 s, before letting the potential return to positive values. On the basis of the above mentioned results, in Figures 2, 3 and 5, the chosen cathodic end potential has proven to be negative enough to sustain the praseodymium and neodymium electrodeposition but not too much to induce lithium deposition. With an increase in deposition time, the maximum peak current at the E_C potential increased, and the charge encompassed by the anodic current waves (A_3 , A_2 , A_1), was substantially enlarged. The increased charge encompassed by anodic current waves with increased deposition time indicated more praseodymium and neodymium metal being dissolved. The conclusion had to be that the electroreduction processes of Nd and Pr in the fluoride bath made of Electrolyte I, on both W and Mo working substrates were taking place in a very similar way.

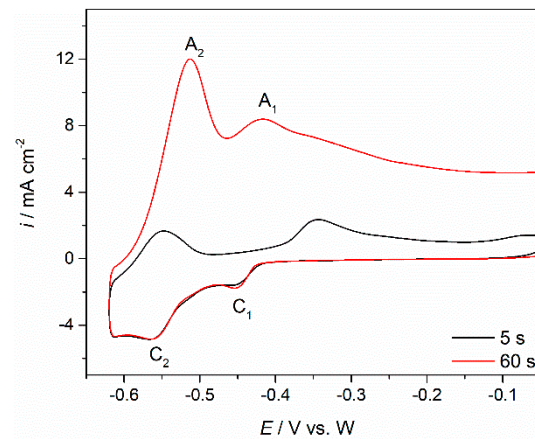


Figure 5. Voltammograms obtained in $\text{NdF}_3 + \text{PrF}_3 + \text{LiF} + 1 \text{ wt.}\% \text{Pr}_6\text{O}_{11} + 1 \text{ wt.}\% \text{Nd}_2\text{O}_3$ melt with different holding times ($\tau = 5$ and 60 s) at negative end potential of the cycle on the Mo working electrode; sweep rate $100 \text{ mV}\cdot\text{s}^{-1}$, temperature 1323 K .

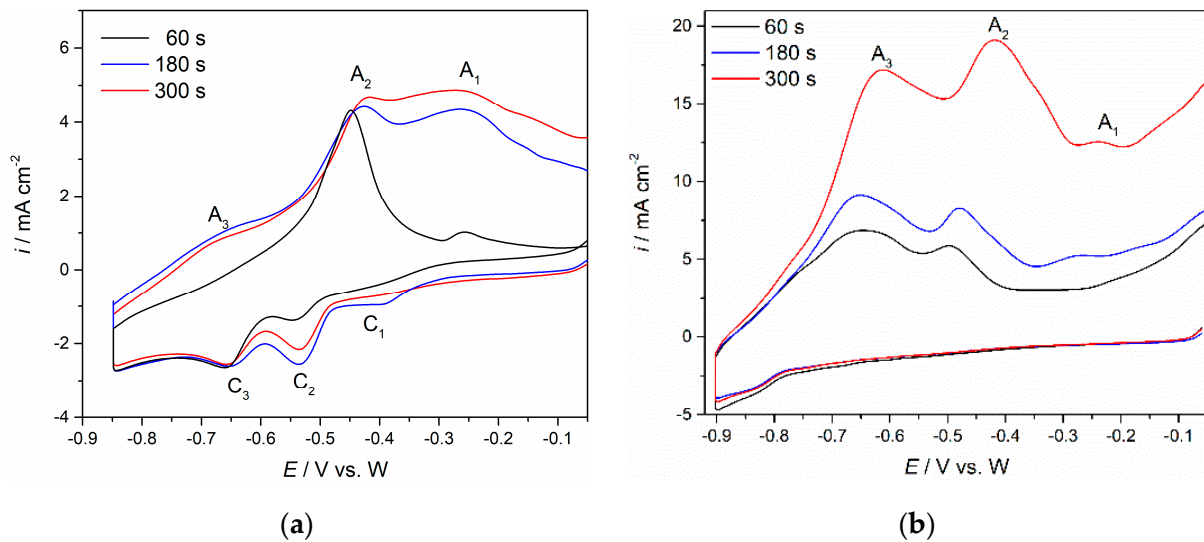


Figure 6. Voltammograms obtained in $\text{NdF}_3 + \text{PrF}_3 + \text{LiF} + 1 \text{ wt.}\% \text{Pr}_6\text{O}_{11} + 1 \text{ wt.}\% \text{Nd}_2\text{O}_3$ melt with different holding times ($\tau = 60, 180$ and 300 s) at negative end potential of the cycle: (a) Mo working electrode, (b) W working electrode, sweep rate $100 \text{ mV}\cdot\text{s}^{-1}$.

To further clarify the electrochemical reduction of neodymium and praseodymium in the molten Electrolyte I, square wave voltammetry (SWV) was employed. SWV is characterised by advanced sensitivity and high resolution and can be applied to estimate the number of exchanged electrons involved in reduction processes [30,31]. A set of square wave voltammograms showing application of different frequencies to the Mo working electrode are presented in Figure 7. The peaks II and III detected at potentials $\approx -0.505 \text{ V}$ vs. W and $\approx -0.640 \text{ V}$ vs. W are in good agreement within the range of the cathodic current wave potentials C_2 and C_3 recorded in the voltammograms presented in Figures 3a and 5a and ascribed to the reduction of $\text{Nd(II)} \rightarrow \text{Nd(0)}$ and $\text{Pr(III)} \rightarrow \text{Pr(0)}$, respectively. For a reversible electrode reaction, mathematical analysis enables us to use a simple equation connecting the width of the half-peak, $W_{1/2}$, recorded in a SW voltammogram with the number of the exchanged electrons [17,30]:

$$W_{1/2} = 3.52RT/nF \quad (1)$$

where $W_{1/2}$ is the half-peak width (V), T is the temperature (K), R represents the universal gas constant ($\text{J}\cdot\text{mol}^{-1}\cdot\text{K}^{-1}$), n is the number of exchanged electrons, and F is the Faraday constant ($96,485 \text{ C}\cdot\text{mol}^{-1}$). Application of Equation (1) for reversible systems is possible if the criterion of linearity for the peak current density vs. the square root of the frequency is fulfilled [17,31]. The linear relationship for the obtained SWV was proven by plotting peak current density vs. the square root of frequency, as can be seen from Figure 7b,c. The relationship can be used to calculate the electrons involved in reactions of the frequency range examined [17,31]. A Gaussian fitting model was applied to calculate the half-peak width, which was used to determine the number of the transferred electrons.

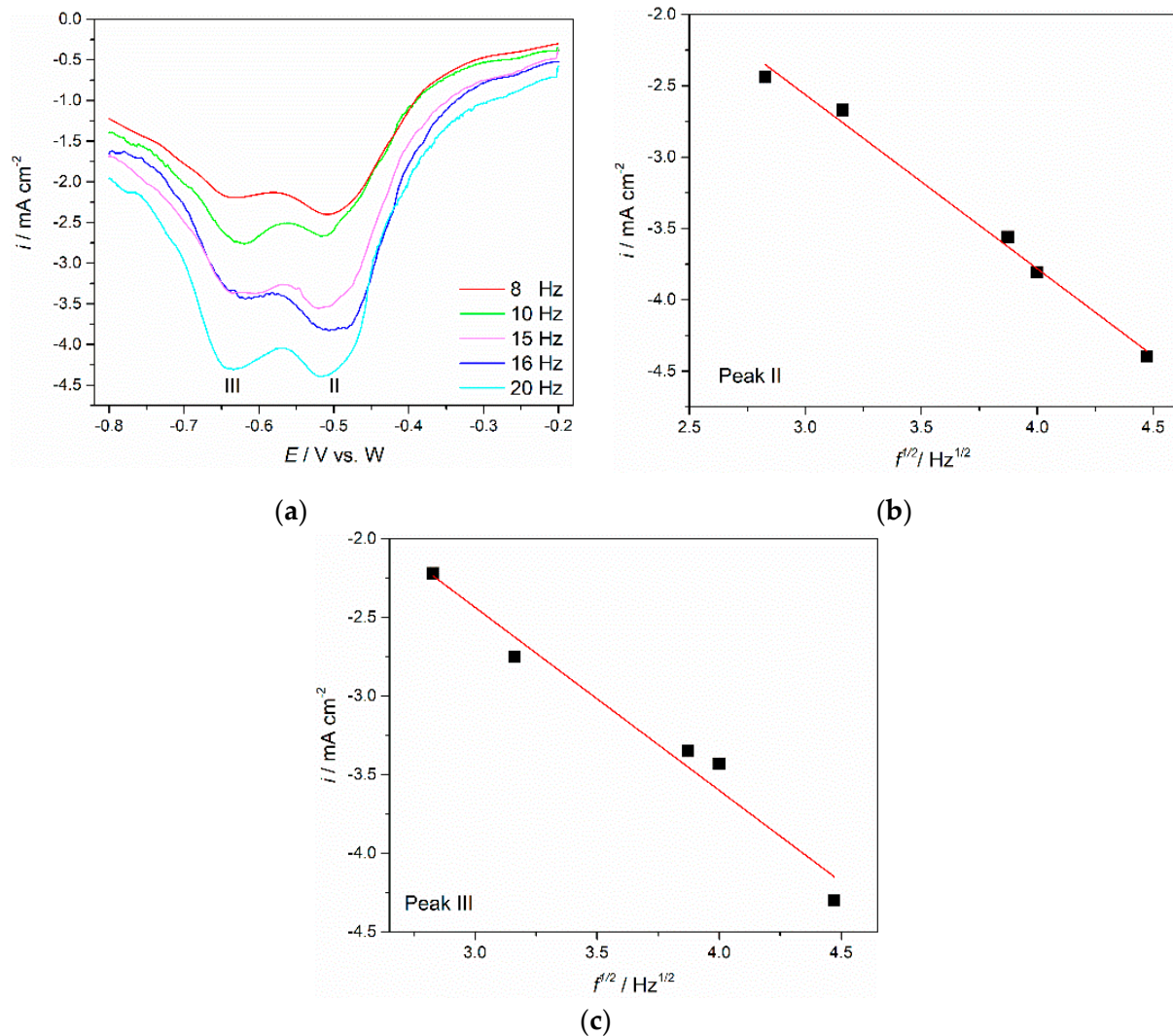


Figure 7. (a) SWV obtained with different frequencies on Mo WE; pulse height: 25 mV; potential step: 1 mV; electrolyte $\text{NdF}_3 + \text{PrF}_3 + \text{LiF} + 1 \text{ wt.}\% \text{Pr}_6\text{O}_{11} + 1 \text{ wt.}\% \text{Nd}_2\text{O}_3$; (b,c) variation of the peak current density vs. the square root of the frequency in Figure 7a for peaks II and III.

The results derived from Equation (1) for peak II revealed the exchange electron number as 2.37, close to 2. The conclusion had to be that the current wave II (C_2) should reflect the reduction of neodymium $\text{Nd}(\text{II})$ into metal Nd , after two electrons were exchanged.

After application of Equation (1) to the current wave III in Figure 7a, it was found that the number of electrons exchanged in the reduction was 3.42, close to 3. This indicated that the reduction of praseodymium, Pr(III) in the used electrolyte takes place in only one electrochemical step involving three electron exchange, namely $\text{Pr(III)} \rightarrow \text{Pr(0)}$. The number of electrons involved in the Pr electroreduction process calculated in the present study corresponds very well with the average oxidation state of Pr in Pr_6O_{11} , which is in alignment to the available data 3.667 [32].

The electrochemical reduction processes of Nd and Pr in Electrolyte I were verified by multiple electrochemical techniques. However, in order to further study the ongoing reaction mechanism, and adjust the deposition parameters to potentially improve the efficiency of the Nd and Pr electrolysis process, the percentage of rare earth oxide that was added to the base electrolyte was changed.

The literature presents claims that increased weight percentage of Nd_2O_3 in the neodymium fluoride electrolyte has a significant impact on Nd metal production [1,22]. Based on our previous work, it appears that better neodymium yield on the cathode is achieved when 2 wt.% of Nd_2O_3 is added to the original neodymium fluoride melt. With the Nd_2O_3 added in the fluoride bath, the oxide will react with NdF_3 or LiF to form different oxyfluorides complexes, namely NdOF or $[\text{NdOF}_5]^{4-}$ [1,12,33,34]. Due to the excess of F^- ions in fluoride molten salts, both complexes coexist, and which complex will be reduced into metallic Nd during the electrodeposition of Nd from Nd(III) depends on the neodymium oxyfluoride/neodymium fluoride ion molar ratio, electrode potential and applied current density [12,34,35]. However, the data on the subject of dissolution of praseodymium oxide, especially Pr_6O_{11} , in fluoride molten bath are rather limited [1,18,25,29]. During preparation of rare earth fluoride electrolytes, praseodymium oxide is dissolved in neodymium fluoride or corresponding praseodymium fluoride molten electrolyte. As a result, of the chemical exchange between the praseodymium oxide and rare earth fluorides, praseodymium oxyfluoride complexes are formed. The knowledge gathered around this subject suggests substantial similarity between the Nd and Pr complexes formed in the melts containing their fluorides, LiF , Nd_2O_3 and Pr_6O_{11} [1,29]. Controlled addition of rare earth oxides to fluoride melts should increase the conductivity of the electrolyte and provide a source of rare earth metals for the electrolysis [18].

Since the objective was to maximize the quantity of Nd and Pr electrodeposited on the working electrode substrates (Mo and W), the experiments were repeated, applying the same set of experimental techniques but in $\text{NdF}_3 + \text{PrF}_3 + \text{LiF} + 2 \text{ wt.}\% \text{Pr}_6\text{O}_{11} + 2 \text{ wt.}\% \text{Nd}_2\text{O}_3$ electrolyte instead. The voltammograms in Figure 8 reflect the results of the CVs applied on a Mo cathode in the Electrolyte II at 1323 K. They exhibit three current waves in the cathodic run (namely C_1 , C_2 and C_3) showing peak potentials at $\approx -0.400 \text{ V}$, $\approx -0.550 \text{ V}$ and $\approx -0.800 \text{ V}$ vs. W, respectively, and three anodic current waves with peak potentials at around $\approx -0.600 \text{ V}$, $\approx -0.350 \text{ V}$ and $\approx -0.200 \text{ V}$ vs. W, respectively. Compared to the voltammograms obtained for Electrolyte I under the same conditions, the current densities recorded were up to five times higher in the electrolyte with higher oxide weight percentages. Otherwise, the current wave pairs C_1/A_1 , C_2/A_2 and C_3/A_3 in Figure 8 should correspond to the electrochemical redox processes, which were found to be Nd(III)/Nd(II) , Nd(II)/Nd(0) and Pr(III)/Pr(0) .

Figure 9 shows CVs similar to those described above for Electrolyte I (Figure 6a,b). These were recorded while applying different holding times at chosen cathodic end potentials, E_C , on Mo working electrode in the electrolyte with higher oxides concentration. By using the same procedures as those employed for Electrolyte I, prolonged deposition at potentials cathodic to the peak potential C_3 induced increased amounts of charge encompassed by the anodic current waves, A_3 and A_2 , which clearly suggested an increased quantity of dissolved praseodymium and neodymium, which were previously deposited during the application of the E_C cathodic potential.

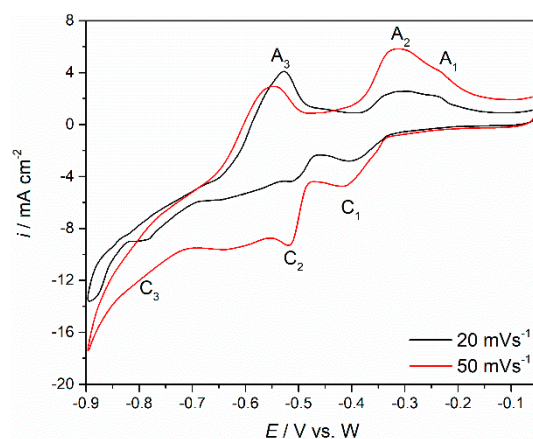


Figure 8. CV recorded on Mo working electrode in molten $\text{NdF}_3 + \text{PrF}_3 + \text{LiF} + 2 \text{ wt.}\% \text{Pr}_6\text{O}_{11} + 2 \text{ wt.}\% \text{Nd}_2\text{O}_3$ electrolyte, from $E_I = -0.050 \text{ V}$ to $E_C = -0.900 \text{ V}$ vs. W; obtained with different scan rates.

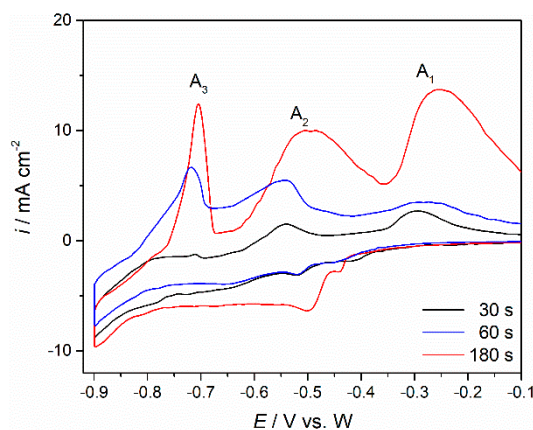


Figure 9. Voltammograms obtained on Mo WE in $\text{NdF}_3 + \text{PrF}_3 + \text{LiF} + 2 \text{ wt.}\% \text{Pr}_6\text{O}_{11} + 2 \text{ wt.}\% \text{Nd}_2\text{O}_3$ melt with different holding times ($\tau = 30, 60$ or 180 s) at negative end potential of the cycle of -0.900 V vs. W; sweep rate $100 \text{ mV}\cdot\text{s}^{-1}$.

To support the proposition that current wave pairs C_1/A_1 , C_2/A_2 and C_3/A_3 recorded in the voltammograms presented in Figures 8 and 9 are the results of praseodymium (C_3/A_3) and neodymium (C_1/A_1 , C_2/A_2), metal phase formation and dissolution open circuit potentiometry was conducted. Nd and Pr were electrodeposited on working electrode substrates by applying a constant potential negative to the peak of the C_3 potential for a short period of time, and then the resulting transient curve for the open circuit working electrode potential was recorded. The open circuit chronopotentiograms obtained in Electrolyte II on a Mo working electrode after potentiostatic electrodeposition at -0.900 V vs. W at 1323 K is presented in Figure 10. The chronopotentiogram shows the plateaux I $\approx -0.750 \text{ V}$, II $\approx -0.600 \text{ V}$ and III $\approx -0.350 \text{ V}$ vs. W, respectively, pointing out that the number of inflection points agreed with the number of anodic current waves (A_1 , A_2 and A_3) seen in the previously presented voltammograms. Relatively stable plateaux I and II reflect two phases (metal Pr and metal Nd) in equilibrium with individual ions in the surrounding electrolyte under the given conditions. The fading potential of the inclined plateau III should reflect declining equilibrium between $\text{Nd(III)} \rightleftharpoons \text{Nd(II)}$ ions.

In the oxide richer Electrolyte II, SWV measurements resulted in more distinct results in terms of the deposition of neodymium and praseodymium. An example of the typical SWV on a Mo working electrode is presented in Figure 11. Two well-pronounced cathodic peaks were recorded in the potential range applied. Half-peak width was established, and after applying a Gaussian fitting model, the exchange electron number was calculated using

Equation (1), after proving the linear relationship; Figure 11b. Reduction peak II identified at around -0.600 V vs. W was processed, and the number of transferred electrons was found to be 2.23, which implied the exchange of two electrons, i.e., the reduction process of Nd(II) into Nd metal. As for the reduction peak III identified at ≈ -0.820 V, the number of exchanged electrons was determined to be 3.43, which can be explained as a three-electron exchange in the one-step reduction process of Pr(III) to Pr metal. SWV obtained with different frequencies on Mo cathode in both electrolytes confirmed the already suggested corresponding potentials of the cathodic reactions C₂ and C₃ and the number of exchanged electrons involved in each reaction.

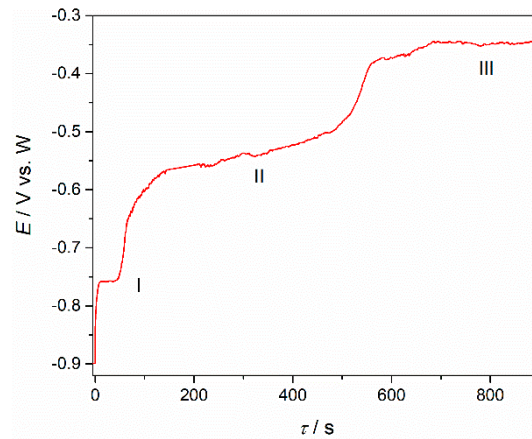


Figure 10. Open circuit potential transient curves obtained on Mo working electrode in molten $\text{NdF}_3 + \text{PrF}_3 + \text{LiF} + 2 \text{ wt.}\% \text{Pr}_6\text{O}_{11} + 2 \text{ wt.}\% \text{Nd}_2\text{O}_3$ electrolyte, after short polarization of 180 s at -0.900 V vs. W.

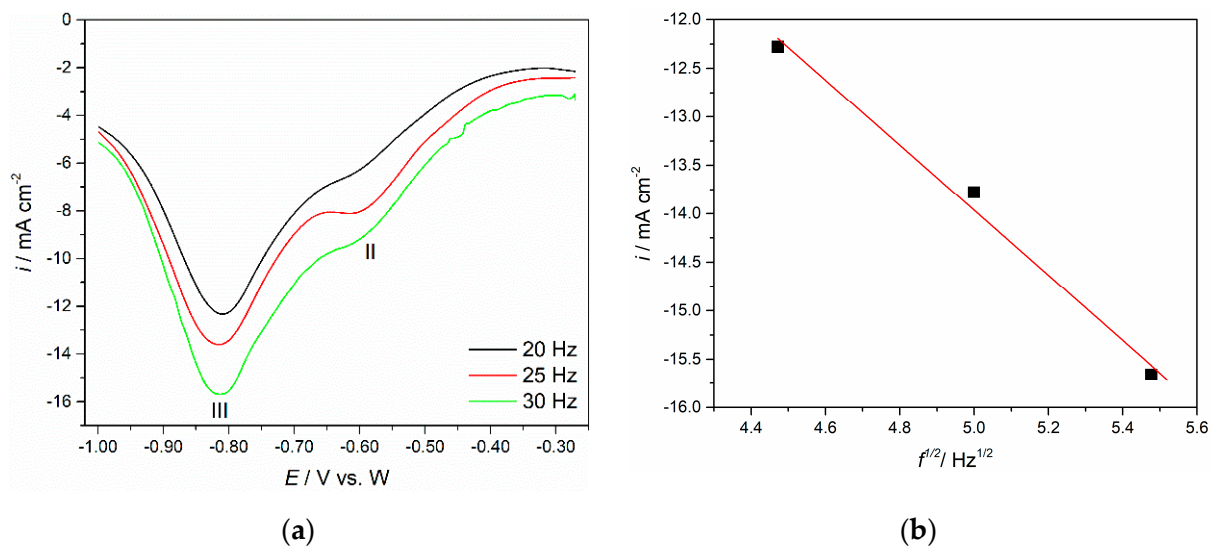


Figure 11. (a) SWV obtained on Mo WE in $\text{NdF}_3 + \text{PrF}_3 + \text{LiF} + 2 \text{ wt.}\% \text{Pr}_6\text{O}_{11} + 2 \text{ wt.}\% \text{Nd}_2\text{O}_3$ electrolyte with different frequency, pulse amplitude = 25 mV, potential step = 1 mV; (b) Variation of the peak current density versus the square root of the frequency in Figure 11a for the peak III.

Thus, taking into account similar behaviour of molybdenum and tungsten in the common Nd-Pr fluoride electrolytes with 2 wt.% and 4 wt.% REO added, one should assume that on both electrodes at potentials more negative than the reduction potential of Pr(III) ions, Nd metal and Pr metal can be co-deposited.

Literature is very scarce regarding Nd and Pr metal being identified on an inert cathode (Mo and W) surface by a deposition similar to the potentiostatic deposition from

an oxide fluoride molten salt electrolyte [25]. There are, however, reports showing Nd and Pr being deposited from fluoride melts, but only in the form of alloys [17,23].

To confirm the presence of Nd and Pr metal on an inert working substrate, potentiostatic electrolysis was conducted at -0.900 V vs. W on Mo working electrode for 60 and 90 min in the electrolyte made of $\text{NdF}_3 + \text{PrF}_3 + \text{LiF} + 2 \text{ wt.}\% \text{Pr}_6\text{O}_{11} + 2 \text{ wt.}\% \text{Nd}_2\text{O}_3$.

The applied potential was approximately 100 mV more negative than the peak potential value of the cathodic current wave C_3 , which reflects the reduction process Pr(III) into Pr(0) ; Figures 2, 5, 6, 8 and 9. After the deposition ended, a solidified electrolyte film from the Mo working electrode surface was mechanically removed. The film-free surface was then analysed by optical microscopy, Figures 12a and 13a, and by XRD, Figures 12b and 13b. The scratches observed were remains of the mechanical preparation of the electrode surface.

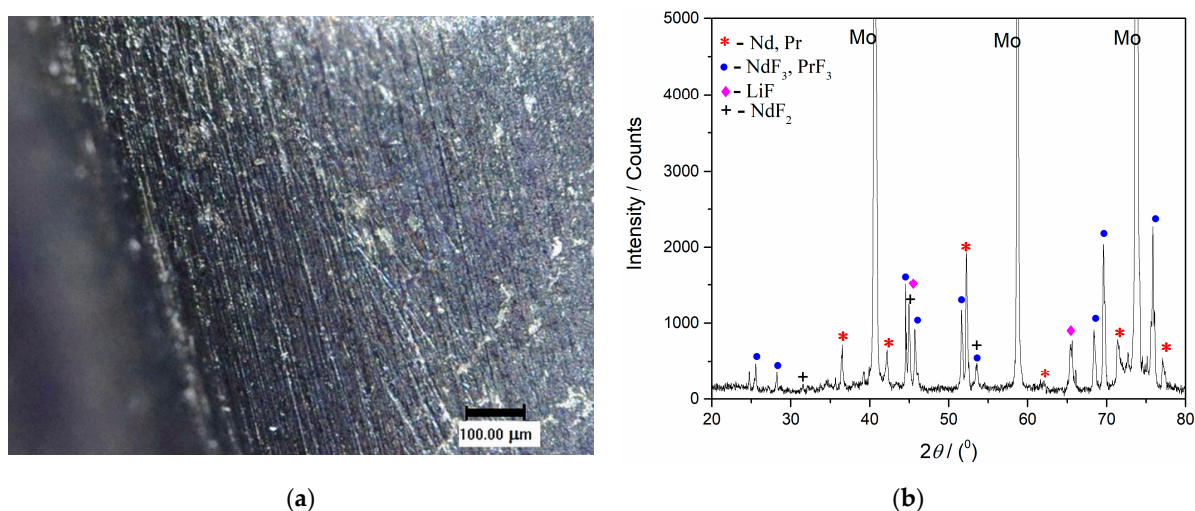


Figure 12. (a) Appearance of the surface of Mo cathode after deposition at -0.900 V vs. W for 60 min, from $\text{NdF}_3 + \text{PrF}_3 + \text{LiF} + 2 \text{ wt.}\% \text{Pr}_6\text{O}_{11} + 2 \text{ wt.}\% \text{Nd}_2\text{O}_3$ electrolyte, at 1323 K; (b) XRD pattern of the Mo working electrode from Figure 12a.

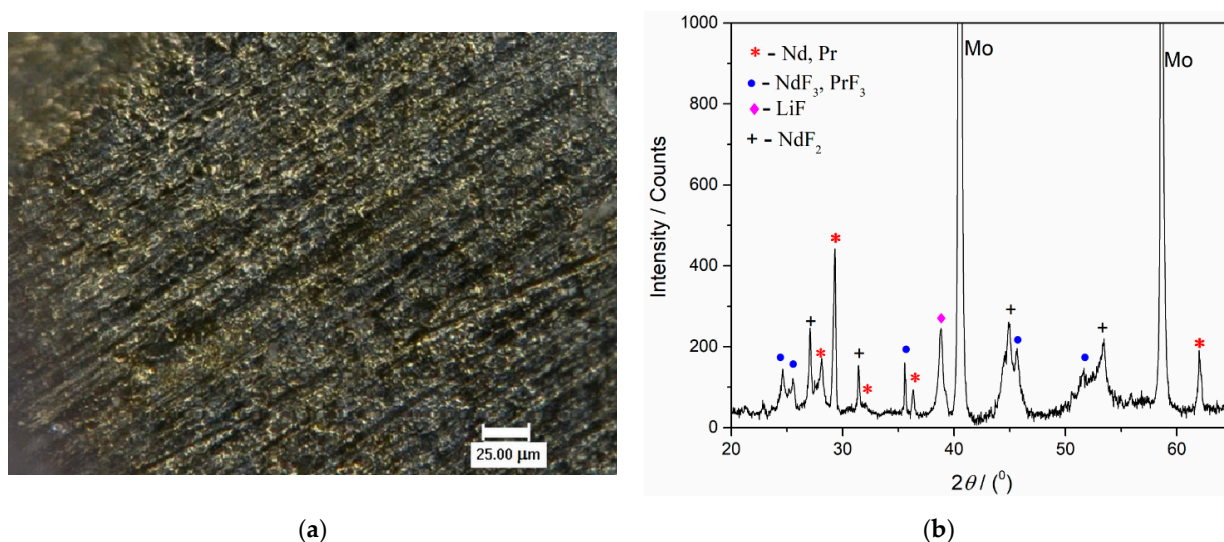


Figure 13. (a) Appearance of the surface of the Mo cathode after deposition at -0.900 V vs. W for 90 min, from molten $\text{NdF}_3 + \text{PrF}_3 + \text{LiF} + 2 \text{ wt.}\% \text{Pr}_6\text{O}_{11} + 2 \text{ wt.}\% \text{Nd}_2\text{O}_3$ electrolyte, at 1323 K. (the solidified electrolyte was removed from the electrode); (b) XRD pattern of the Mo working electrode from Figure 13a.

Figure 12b presents the XRD pattern of the sample obtained after deposition at a constant potential of -0.900 V vs. W for 60 min in molten Electrolyte II. Peaks identified in the diffractogram at $2\theta = 36.40^\circ, 41.83^\circ, 52.37^\circ, 62.37^\circ, 71.75^\circ, 77.33^\circ$ are attributed to

hexagonal Nd [JCPDS No. 03-065-3424], and the peaks with slight variations in 2θ values, due to very similar lattice parameters of both metals, at 36.27° , 411.89° , 52.14° , 62.16° , 71.45° , 77.01° are characteristic of hexagonal Pr [JCPDS No. 01-089-2921]. The diffraction peaks identified at $2\theta = 25.31^\circ$, 28.23° , 44.61° , 45.73° , 51.66° , 53.63° , 68.35° , 68.78° , 75.55° , are characteristic of hexagonal NdF_3 [JCPDS No. 01-078-1859] and hexagonal PrF_3 [JCPDS No. 01-078-1464], respectively. The diffraction peaks recorded at $2\theta = 45.06^\circ$ and 65.63° belong to face-centered cubic LiF [JCPDS No. 01-072-1538]. The peak at a 2θ value of 31.47° reflects face-centered cubic NdF_2 and the peaks at around 45.1° and 53.5° can also be ascribed to NdF_2 [JCPDS No. 00-033-0934].

With the XRD patterns presented in Figures 12b and 13b, the electrodeposition of Nd and Pr on an inert electrode used was confirmed. However, the presence of NdF_2 , NdF_3 , PrF_3 and LiF melt residue could not be avoided.

With prolonged deposition time, in addition to those already seen in Figure 12b, new prominent peaks corresponding to Nd and Pr metals could be seen in the diffractogram in Figure 13b. They appear at 2θ values of 28.16° , 29.18° , and 32.06° , which correspond to Nd, and at very similar 2θ values— 28.05° , 29.06° , and 31.94° —corresponding to the Pr metal.

The results of the electrochemical measurements and XRD analysis revealed that the chosen potential at -0.900 V vs. W was cathodic enough to sustain Nd and Pr metal deposition (deposition current density of ≈ -6 mAcm^{-2}) without lithium being co-deposited, see Figures 12b and 13b.

Concerning XRD NdF_2 identification, it should be mentioned that very similar results were obtained on the Mo working electrode after potentiostatic electrodeposition from the molten salt $\text{NdF}_3 + \text{LiF} + 2$ wt.% Nd_2O_3 electrolyte [12,15]. It seems that NdF_2 is formed as a result of disproportionate reaction between Nd metal electrodeposited and Nd(III) ions: $\text{Nd}(0) + 2\text{Nd}(\text{III}) \rightarrow 3\text{Nd}(\text{II})$. These results were also in agreement with the conclusions obtained by some other authors describing neodymium electrodeposition from neodymium oxyfluoride melts, at temperatures close to or above 1323 K [12,15,20].

However, there is also the aspect of ecologically unacceptable gases that could evolve on the working glassy carbon anode during Nd and Pr electrodeposition onto inert Mo or W cathode from used molten salts electrolytes. To make an assessment of this potential result, anodic gases evolved during the controlled potentiostatic electrolysis and electrochemical measurements were analysed in situ by FTIR spectrometer.

Recent literature reports that the formation of greenhouse gasses is influenced by the concentration of REO dissolved in the fluoride electrolyte [8,12,24,36]. In a molten oxide fluoride electrolyte with a given oxide concentration, where glassy carbon serves as the anode during potentiostatic electrolysis, the generated oxygen species react with the carbon anode and produce mainly CO and CO_2 . When the REO concentration drops off, the “anode effect” occurs and perfluorocarbon (PFC) gases such as CF_4 and C_2F_6 are generated, and their greenhouse gas potential is much higher, exceeding 7390 and 12,200 CO_2 -equivalents, respectively [25,36,37]. However, it should be noted that the formation of PFC gases occurs at significantly higher anodic potentials than the CO/ CO_2 formation [8]. Thus, for an environmentally friendly electrolytic production of Nd-Pr alloys, apart from the controlled potentiostatic mode, the right amount of RE oxides in the electrolyte is needed in order to avoid the critical conditions for CF_4 and C_2F_6 gas production [1,8,12,24,36,37].

Composition of off-gases during the electrochemical measurements and electrolysis in this work was recorded in situ and ratio and quantity of evolved gases were detected, see Figure 14. It was noticed that throughout the electrochemical experiments, CO and CO_2 gases were detected, and except for some spikes during replacement of the electrode, the average quantity of CO was below 100 ppm and for CO_2 around 5 ppm. However, during the potentiostatic Pr/Nd deposition, CO quantity evolved was higher, being around 700 ppm on average, with maximum recorded ≈ 1200 ppm. Evolved quantity of CO_2 was around 200 ppm during the deposition. The results indicate that within the controlled potential range applied, the electrodeposition of Nd/Pr proceeds at the expense of the

neodymium and praseodymium oxides [24]. The anodic working potentials, governed by the applied cathodic potentials were obviously high enough to sustain oxidation processes on the GC anode by oxygen and fluoride ions at longer reaction times, prior to the partial passivation of the anode occurs. Similar observation was reported by other researchers in the field, claiming that only oxygen containing species are taking part in partial passivation and CF_4 emission starts only later at higher anodic potentials [24].

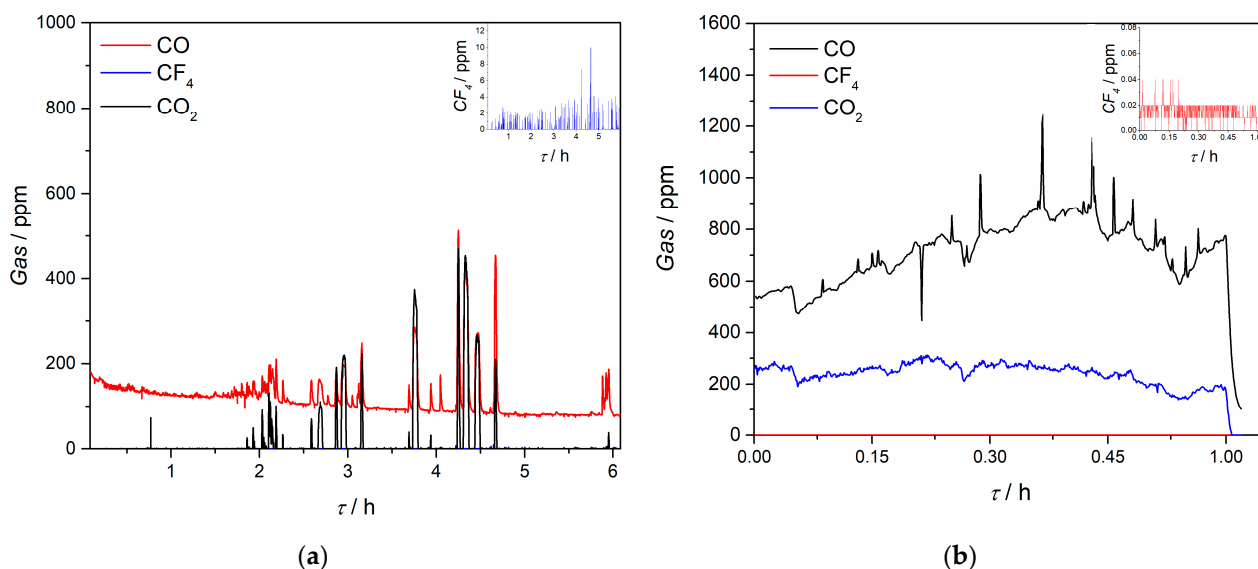


Figure 14. Off-gas generated on the GC anode recorded in situ with an FTIR spectrometer during: (a) electrochemical experiments; (b) potentiostatic deposition at -0.900 V vs. W; insert are measurements for CF_4 off-gas; working electrode Mo, in $\text{NdF}_3 + \text{PrF}_3 + \text{LiF} + 2$ wt.% $\text{Pr}_6\text{O}_{11} + 2$ wt.% Nd_2O_3 electrolyte, $T = 1323$ K.

The quantity of recorded CF_4 was almost negligible; the average values during the electrochemical experiments were below 5 ppm and during the potentiostatic Pr/Nd deposition around 0.02 ppm, which should be attributed to the relatively low applied deposition overpotential (and therefore small anodic overpotential). At the same time, C_2F_6 was not detected under the potential regime applied. According to Zhang et al. [38], and taking into account the off-gas results obtained during voltammetry measurements in this study, it appears that in the positive scan the PFC gases are being adsorbed on the anode and are forming an insulating layer which reduces the anode oxidation current. During the reverse scan PFC are rapidly desorbed from the graphite anode and the desorption potential is more negative than the adsorption potential, thus reducing the PFC emission to a great extent and keeping the process in a green process window [38,39].

4. Conclusions

(1) Praseodymium and neodymium were successfully electrodeposited from $\text{NdF}_3 + \text{PrF}_3 + \text{LiF} + 1$ wt.% $\text{Pr}_6\text{O}_{11} + 1$ wt.% Nd_2O_3 and $\text{NdF}_3 + \text{PrF}_3 + \text{LiF} + 2$ wt.% $\text{Pr}_6\text{O}_{11} + 2$ wt.% Nd_2O_3 molten electrolytes at 1323 K on inert Mo and W electrodes. The results recorded by electrochemical techniques confirm that optimal conditions for the co-deposition were constant overpotential of ≈ -0.100 V of praseodymium deposition potential (-0.700 V to -0.800 V vs. W on Mo electrode and -0.750 V to -0.850 V vs. W on W electrode), which should provide deposition current densities of around 6 mAcm^{-2} in the fluoride molten salt.

(2) Analysis of the results obtained by applied electrochemical techniques have shown that praseodymium deposition proceeds in one step involving three electrons exchange ($\text{Pr(III)} \rightarrow \text{Pr(0)}$). The same techniques previously confirmed earlier propositions that neodymium deposition includes two steps: the first involving exchange of one electron ($\text{Nd(III)} \rightarrow \text{Nd(II)}$) and the second involving exchange of two electrons ($\text{Nd(II)} \rightarrow \text{Nd(0)}$).

(3) It was established that Pr and Nd co-deposition performed under relatively small praseodymium deposition overpotentials in the used electrolytes and at applied temperatures on the inert Mo and W cathodes was very successful because: (a) lithium deposition was disabled, and (b) it allowed only very small evolution of the greenhouse gases due to the low anodic potential.

(4) Such low levels of carbon oxides, fluorine and fluorocarbon gas evolution from the glassy carbon anode indicates this process to be an environmentally friendly technique for rare earth metal deposition. Thus, this process has the potential to recycle the rare earth elements of a neodymium iron boron magnet if they are first separated from the magnet in oxide form. If Nd and Pr are deposited simultaneously as an alloy without emitting a large amount of greenhouse gases, it should be possible to use this alloy directly in magnet production.

Author Contributions: V.S.C. methodology; writing—original draft preparation; D.F. performed most of the experiments; N.M.V. investigation; writing—original draft preparation; T.S.B. XRD data curation; B.F. and J.N.J. helped with the corrections of the manuscript and supervised; B.F. from RWTH Aachen University provided funding for publication. All authors discussed the results and commented on the manuscript. All authors have read and agreed to the published version of the manuscript.

Funding: Part of this research was supported by the funds of the bilateral research project (ID:451-03-01344/2020-09/8), supported by the Ministry of Education, Science and Technological Development of the Republic of Serbia and German Academic Exchange Service (DAAD).

Institutional Review Board Statement: Not applicable.

Informed Consent Statement: Not applicable.

Data Availability Statement: Not applicable.

Acknowledgments: Vesna S. Cvetković and Nataša M. Vukićević acknowledge the financial support for the investigation received from the Ministry of Education, Science and Technological Development of the Republic of Serbia (Grant No.451-03-9/2021-14/200026).

Conflicts of Interest: The authors declare no conflict of interest.

References

1. Sarfo, P.; Das, A.; Young, C. Extraction and Optimization of Neodymium from Molten Fluoride Electrolysis. *Sep. Purif. Technol.* **2020**, *256*, 117770. [[CrossRef](#)]
2. Joo, M.H.; Park, S.J.; Hong, S.-M.; Rhee, C.K.; Kim, D.; Sohn, Y. Electrodeposition and Characterization of Lanthanide Elements on Carbon Sheets. *Coatings* **2021**, *11*, 100. [[CrossRef](#)]
3. Joo, M.H.; Park, S.J.; Hong, S.M.; Rhee, C.K.; Sohn, Y. Electrochemical Recovery and Behaviors of Rare Earth (La, Ce, Pr, Nd, Sm, Eu, Gd, Tb, Dy, Ho, Er, Tm, and Yb) Ions on Ni Sheets. *Materials* **2020**, *13*, 5314. [[CrossRef](#)]
4. Kaya, E.; Kaya, O.; Stopic, S.; Gürmen, S.; Friedrich, B. NdFeB Magnets Recycling Process: An Alternative Method to Produce Mixed Rare Earth Oxide from Scrap NdFeB Magnets. *Metals* **2021**, *11*, 716. [[CrossRef](#)]
5. Yasuda, K.; Kondo, K.; Nohira, T.; Hagiwara, R. Electrochemical Formation of Pr–Ni Alloys in LiF–CaF₂–PrF₃ and NaCl–KCl–PrCl₃ Melts. *J. Electrochem. Soc.* **2014**, *161*, D3097–D3104. [[CrossRef](#)]
6. Yang, Y.; Walton, A.; Sheridan, R.; Güth, K.; Gauß, R.; Gutfleisch, O.; Buchert, M.; Steenari, B.-M.; Van Gerven, T.; Jones, P.T.; et al. REE Recovery from End-of-Life NdFeB Permanent Magnet Scrap: A Critical Review. *J. Sustain. Met.* **2016**, *3*, 122–149. [[CrossRef](#)]
7. Stopic, S.; Friedrich, B. Advances in Understanding of the Application of Unit Operations in Metallurgy of Rare Earth Elements. *Metals* **2021**, *11*, 978. [[CrossRef](#)]
8. Senanu, S.; Ratvik, A.; Gudbrandsen, H.; Martinez, A.; Støre, A.; Gebarowski, W. Dissolution and Online Monitoring of Nd and Pr Oxides in NdF₃–PrF₃–LiF Electrolytes. *Metals* **2021**, *11*, 326. [[CrossRef](#)]
9. Riaño, S.; Binnemans, K. Extraction and separation of neodymium and dysprosium from used NdFeB magnets: An application of ionic liquids in solvent extraction towards the recycling of magnets. *Green Chem.* **2015**, *17*, 2931–2942. [[CrossRef](#)]
10. Tang, H.; Yan, Y.-D.; Zhang, M.-L.; Li, X.; Huang, Y.; Xu, Y.-L.; Xue, Y.; Han, W.; Zhang, Z.-J. AlCl₃-aided extraction of praseodymium from Pr₆O₁₁ in LiCl–KCl eutectic melts. *Electrochim. Acta* **2012**, *88*, 457–462. [[CrossRef](#)]
11. Hua, Z.; Liu, H.; Wang, J.; He, J.; Xiao, S.; Xiao, Y.; Yang, Y. Electrochemical Behavior of Neodymium and Formation of Mg–Nd Alloys in Molten Chlorides. *ACS Sustain. Chem. Eng.* **2017**, *5*, 8089–8096. [[CrossRef](#)]
12. Cvetković, V.S.; Feldhaus, D.; Vukićević, N.M.; Barudžija, T.S.; Friedrich, B.; Jovićević, J.N. Investigation on the Electrochemical Behaviour and Deposition Mechanism of Neodymium in NdF₃–LiF–Nd₂O₃ Melt on Mo Electrode. *Metals* **2020**, *10*, 576. [[CrossRef](#)]

13. Nohira, T.; Kobayashi, S.; Kondo, K.; Yasuda, K.; Hagiwara, R.; Oishi, T.; Konishi, H. Electrochemical Formation of RE-Ni (RE = Pr, Nd, Dy) Alloys in Molten Halides. *ECS Trans.* **2013**, *50*, 473–482. [[CrossRef](#)]
14. Liu, K.; Liu, Y.-L.; Chai, Z.-F.; Shi, W.-Q. Evaluation of the Electroextractions of Ce and Nd from LiCl-KCl Molten Salt Using Liquid Ga Electrode. *J. Electrochem. Soc.* **2017**, *164*, D169–D178. [[CrossRef](#)]
15. Cvetković, V.S.; Vukićević, N.M.; Feldhaus, D.; Barudžija, T.S.; Stevanović, J.; Friedrich, B.; Jovičić, J.N. Study of Nd Deposition onto W and Mo Cathodes from Molten Oxide-Fluoride Electrolyte. *Int. J. Electrochem. Sci.* **2020**, *15*, 7039–7052. [[CrossRef](#)]
16. Castrillejo, Y.; Bermejo, M.; Arocas, P.D.; Martínez, A.; Barrado, E. The electrochemical behaviour of the Pr(III)/Pr redox system at Bi and Cd liquid electrodes in molten eutectic LiCl–KCl. *J. Electroanal. Chem.* **2005**, *579*, 343–358. [[CrossRef](#)]
17. Yang, Y.; Lan, C.; Guo, L.; An, Z.; Zhao, Z.; Li, B. Recovery of rare-earth element from rare-earth permanent magnet waste by electro-refining in molten fluorides. *Sep. Purif. Technol.* **2019**, *233*, 116030. [[CrossRef](#)]
18. Zhang, Y.N.; Li, J.; Chai, D.P.; Gao, Y.Y.; Wang, C.Z.; Hou, G.H.; Yu, Q.; Liu, L.Y.; Zhang, F.P.; Liu, X. Study on the Conductivity of Molten Salt in $\text{PrF}_3\text{-NdF}_3\text{-LiF-Pr}_6\text{O}_{11}\text{-Nd}_2\text{O}_3$. *Chin. Rare Earths* **2020**, *41*, 92–96.
19. Yasuda, K.; Kondo, K.; Kobayashi, S.; Nohira, T.; Hagiwara, R. Selective Formation of Rare Earth-Nickel Alloys via Electrochemical Reactions in NaCl-KCl Molten Salt. *J. Electrochem. Soc.* **2016**, *163*, D140. [[CrossRef](#)]
20. Huang, C.; Liu, X.; Gao, Y.; Liu, S.; Li, B. Cathodic processes of neodymium(III) in $\text{LiF-NdF}_3\text{-Nd}_2\text{O}_3$ melts. *Faraday Discuss.* **2016**, *190*, 339–349. [[CrossRef](#)] [[PubMed](#)]
21. Stefanidaki, E.; Hasiotis, C.; Kontoyannis, C. Electrodeposition of neodymium from $\text{LiF-NdF}_3\text{-Nd}_2\text{O}_3$ melts. *Electrochim. Acta* **2001**, *46*, 2665–2670. [[CrossRef](#)]
22. Guo, X.; Sun, Z.; Sietsma, J.; Yang, Y. Semiempirical Model for the Solubility of Rare Earth Oxides in Molten Fluorides. *Ind. Eng. Chem. Res.* **2016**, *55*, 4773–4781. [[CrossRef](#)]
23. Morrice, E.; Henrie, T.A. *Electrowinning High-Purity Neodymium, Praseodymium, and Didymium Metals from Their Oxides*; U.S. Patent, Report number BM-RI-6957; Bureau of Mines: Washington, DC, USA, 1 January 1967.
24. Milicevic, K.; Feldhaus, D.; Friedrich, B. Conditions and Mechanisms of Gas Emissions from Didymium Electrolysis and Its Process Control. In *Light Metals 2018*; Springer: Cham, Switzerland, 2018; pp. 1435–1441. [[CrossRef](#)]
25. Milicevic, K.; Friedrich, B. Special Feature: Electrowinning of didymium. *Appl. Mineral. Bull. Appl. Mineral. Gr.* **2017**, *2*.
26. Yi, Y.; Weinberg, G.; Prenzel, M.; Greiner, M.; Heumann, S.; Becker, S.; Schlögl, R. Electrochemical corrosion of a glassy carbon electrode. *Catal. Today* **2017**, *295*, 32–40. [[CrossRef](#)]
27. Yuan, Y.; Li, W.; Chen, H.; Wang, Z.; Jin, X.; Chen, G.Z. Electrolysis of metal oxides in MgCl_2 based molten salts with an inert graphite anode. *Faraday Discuss.* **2016**, *190*, 85–96. [[CrossRef](#)]
28. Straka, M.; Korenko, M.; Szatmáry, L. Electrochemistry of praseodymium in LiF-CaF_2 . *J. Radioanal. Nucl. Chem.* **2011**, *289*, 591–593. [[CrossRef](#)]
29. Ghandehari, M.H. Electrolytic Production of Praseodymium. U.S. Patent 4627898, 1986.
30. Osteryoung, J.G.; Osteryoung, R.A. Square Wave Voltammetry. *Anal. Chem.* **1985**, *57*, 101A–110A. [[CrossRef](#)]
31. Mirceski, V.; Skrzypek, S.; Stojanov, L. Square-wave voltammetry. *Chem. Texts* **2018**, *4*, 17. [[CrossRef](#)]
32. Ferro, S. Physicochemical and Electrical Properties of Praseodymium Oxides. *Int. J. Electrochem.* **2011**, *2011*, 561204. [[CrossRef](#)]
33. Hu, X.; Wang, Z.; Gao, B.; Shi, Z.; Liu, F.; Cao, X. Density and ionic structure of $\text{NdF}_3\text{-LiF}$ melts. *J. Rare Earths* **2010**, *28*, 587–590. [[CrossRef](#)]
34. Ciomag, M.; Gibilaro, M.; Massot, L.; Laucournet, R.; Chamelot, P. Neodymium electrowinning into copper-neodymium alloys by mixed oxide reduction in molten fluoride media. *J. Fluor. Chem.* **2016**, *184*, 1–7. [[CrossRef](#)]
35. Kaneko, A.; Yamamoto, Y.; Okada, C. Electrochemistry of rare earth fluoride molten salts. *J. Alloys Compd.* **1993**, *193*, 44–46. [[CrossRef](#)]
36. Vogel, H.; Flerus, B.; Stoffner, F.; Friedrich, K.B. Reducing Greenhouse Gas Emission from the Neodymium Oxide Electrolysis. Part I: Analysis of the Anodic Gas Formation. *J. Sustain. Met.* **2016**, *3*, 99–107. [[CrossRef](#)]
37. Vogel, H.; Friedrich, B. Reducing Greenhouse Gas Emission from the Neodymium Oxide Electrolysis. Part II: Basics of a Process Control Avoiding PFC Emission. *Int. J. Nonferrous Met.* **2017**, *06*, 27–46. [[CrossRef](#)]
38. Zhang, L.; Wang, X.; Gong, B. Perfluorocarbon emissions from electrolytic reduction of rare earth metals in fluoride/oxide system. *Atmos. Pollut. Res.* **2018**, *9*, 61–65. [[CrossRef](#)]
39. Liu, S.; Chen, L.; Li, B.; Wang, L.; Yan, B.; Liu, M. Anode processes for Nd electrowinning from $\text{LiF-NdF}_3\text{-Nd}_2\text{O}_3$ melt. *Electrochim. Acta* **2014**, *147*, 82–86. [[CrossRef](#)]